

---

# SAGOnline: Segment Any Gaussians Online

---

**Wentao Sun**

University of Waterloo  
N2L 3G1 Waterloo, Canada  
w27sun@uwaterloo.ca

**Quanyun Wu**

University of Waterloo  
N2L 3G1 Waterloo, Canada  
q34wu@uwaterloo.ca

**Hanqing Xu**

East China Normal University  
200050, Shanghai, China  
51273901140@stu.ecnu.edu.cn

**Kyle Gao**

University of Waterloo  
N2L 3G1 Waterloo, Canada  
y56gao@uwaterloo.ca

**Zhengsen Xu**

University of Calgary  
T2N 1N4 Calgary, Canada  
zhengsen.xu@ucalgary.ca

**Yiping Chen**

Sun Yat-Sen University  
519082 Zhuhai, China  
chenyp79@mail.sysu.edu.cn

**Dedong Zhang**

University of Waterloo  
N2L 3G1 Waterloo, Canada  
dedong.zhang@uwaterloo.ca

**Lingfei Ma**

East China Normal University  
200050, Shanghai, China  
153ma@cufe.edu.cn

**John S. Zelek**

University of Waterloo  
N2L 3G1 Waterloo, Canada  
jzelek@uwaterloo.ca

**Jonathan Li**

University of Waterloo  
N2L 3G1 Waterloo, Canada  
junli@uwaterloo.ca

## Abstract

3D Gaussian Splatting (3DGS) has emerged as a powerful paradigm for explicit 3D scene representation, yet achieving efficient and consistent 3D segmentation remains challenging. Current methods suffer from prohibitive computational costs, limited 3D spatial reasoning, and an inability to track multiple objects simultaneously. We present Segment Any Gaussians Online (SAGOnline), a lightweight and zero-shot framework for real-time 3D segmentation in Gaussian scenes that addresses these limitations through two key innovations: (1) a decoupled strategy that integrates video foundation models (e.g., SAM 2) for view-consistent 2D

mask propagation across synthesized views; and (2) a GPU-accelerated 3D mask generation and Gaussian-level instance labeling algorithm that assigns unique identifiers to 3D primitives, enabling lossless multi-object tracking and segmentation across views. SAGOnline achieves state-of-the-art performance on NVOS (92.7% mIoU) and Spin-NeRF (95.2% mIoU) benchmarks, outperforming Feature3DGS, OmniSeg3D, and SA3D by 15–1500× in inference speed (27 ms/frame). Qualitative results demonstrate robust multi-object segmentation and tracking in complex scenes. Our contributions include: (i) a lightweight and zero-shot framework for 3D segmentation in Gaussian scenes, (ii) explicit labeling of Gaussian primitives enabling simultaneous segmentation and tracking, and (iii) the effective adaptation of 2D video foundation models to the 3D domain. This work allows real-time rendering and 3D scene understanding, paving the way for practical AR/VR and robotic applications.

## 1 Introduction

Neural Radiance Fields (NeRF) [1] have revolutionized 3D scene reconstruction and novel view synthesis through implicit neural representations. The recent emergence of 3D Gaussian Splatting (3DGS) [2] marks a significant milestone, offering explicit scene representation with remarkable rendering speed and visual quality.

Compared to NeRF’s volumetric rendering approach, 3DGS achieves superior efficiency through anisotropic splatting of learnable Gaussians while maintaining competitive reconstruction accuracy.

This explicit representation paradigm creates new opportunities for 3D understanding tasks, particularly in cross-view consistent segmentation. Such capabilities are critical for applications in augmented reality [3–5], robotic manipulation [6–8], and autonomous systems [9, 10], where real-time 3D scene parsing is essential. Both NeRF- and 3DGS-based methods aim to achieve image segmentation that remains consistent across novel views [11–18].

Recent advances in 3D segmentation primarily follow three paradigms: distillation-based, contrastive learning-based and direct manipulation approaches. The former, exemplified by Feature3DGS [14], distills 2D segmentation features into 3D representations through feature projection and aggregation. The latter, represented by OmniSeg3D [15], leverages contrastive learning to align 3D structures with the outputs of 2D foundation models. However, these two kinds of method suffer from three critical challenges that hinder practical deployment.

The first challenge is the prohibitive computational costs during either training or inference. Methods like SA3D [19] require over 30 seconds per view due to iterative refinement with 2D foundation models, while distillation- and contrastive learning-based solutions like Feature3DGS and OmniSeg3D demand 20-40 minutes of additional training for 3D feature alignment. This inefficiency stems from their reliance on per-frame processing and high-dimensional feature optimization.

The second challenge is an efficient way to get comprehensive global 3D segmentation results, such as complete 3D masks. This limitation stems from their inherently 2D formulation of the multi-view consistent segmentation problem. While some methods can efficiently segment target objects in novel views and produce corresponding 2D masks, they lack one efficient and simple way to generate unified 3D segmentation masks that coherently represent the entire 3D scene.

Third, it is consistent multi-object segmentation and tracking across multiple views. Specifically, assigning unique identifiers to individual objects in multi-object scenarios and maintaining segmentation consistency across viewpoints are challenging. This deficiency arises because current algorithms [14, 16, 15, 17] were primarily designed for single-object segmentation. When confronted with multiple target objects, these methods cannot automatically track and segment each instance with persistent IDs across different views. Consequently, users must repeatedly provide new prompts to segment different objects in novel views, significantly limiting their practical utility.

Direct manipulation approaches [20, 21] operate directly on Gaussian primitives. For example, GaussianCut [20] leverages temporally consistent 2D segmentation masks provided by video models and combines them with a graph cut algorithm to explicitly model the relationships between Gaussian primitives. This training-free approach utilizes the mapping between Gaussian primitives and images to achieve segmentation, resulting in significantly higher algorithmic efficiency compared to the first

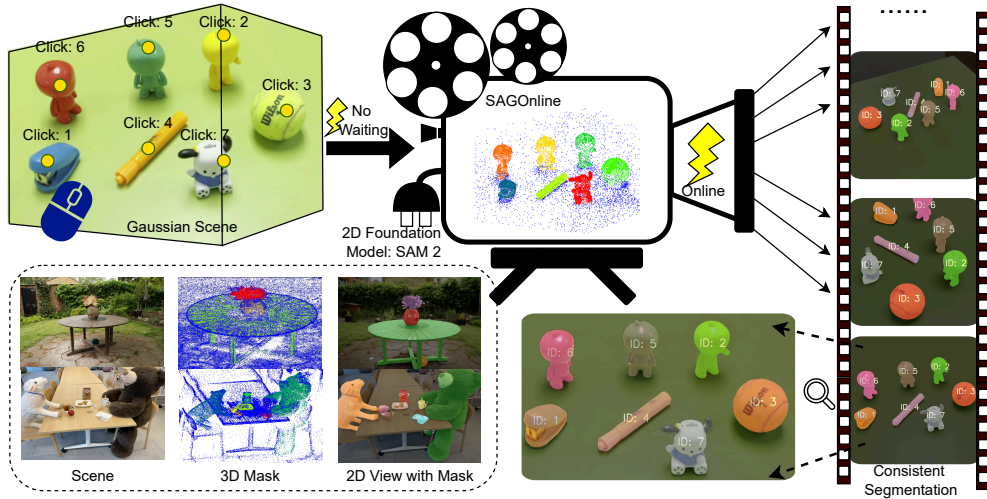


Figure 1: We propose **SAGOnline**, a lightweight and zero-shot framework for real-time 3D segmentation in Gaussian scenes. SAGOnline achieves 27 ms/frame inference by decoupling the task into view-consistent 2D segmentation (via video foundation models like SAM 2) and GPU-accelerated 3D mask generation. It uniquely supports real-time, multi-object tracking through Gaussian-level instance identifiers while requiring zero training.

two categories. However, these methods still have room for improvement in terms of segmentation accuracy.

To address all these challenges simultaneously, we propose Segment Any Gaussians Online (SAGOnline), a lightweight and zero-shot framework that achieves real-time 3D segmentation (27 ms/frame) in Gaussian scenes through two key innovations: 1) We decouple the problem into view-consistent 2D segmentation and Gaussian-level 3D segmentation. Novel view segmentation leverages video foundation models (e.g., Segment Anything Model 2 (SAM 2) [22]) to propagate masks across synthesized views, enabling real-time, training-free segmentation. 2) We design a GPU-accelerated algorithm that rapidly transforms 2D masks into 3D masks and assigns unique identifiers to each Gaussian primitive. Using these identifiers, our method achieves multi-view consistent segmentation that outperforms existing approaches in speed and enables lossless, simultaneous segmentation and tracking of multiple objects.

Extensive experiments demonstrate state-of-the-art (SOTA) performance on the NVOS [11] and Spin-NeRF [12] benchmarks, achieving 92.7% and 95.2% mIoU, respectively. SAGOnline also outperforms existing methods including: Feature3dgs [14], OmniSeg3D-gs [15], GARField [17], and SA3D [19]—by 15-1500 $\times$  in inference speed while requiring zero training time. Qualitative results showcase robust multi-object tracking and segmentation in complex scenes. Our key contributions include: 1) A lightweight and zero-shot framework for 3D segmentation in Gaussian scenes; 2) Explicit instance labeling enabling that enables simultaneous multi-object tracking; 3) Extension of video foundation models (e.g., SAM 2) to the 3D domain.

## 2 Related Work

### 2.1 3D Gaussian Representations

Recent advancements in 3D Gaussian Splatting (3DGS) can be categorized into seven primary research directions: sparse input [23–27], memory efficiency [28–30], photorealism [31–34], improved optimization algorithms [35–39], extra properties [14, 18, 40, 41], hybrid representation [42–44], and novel rendering algorithms [45, 46]. [47]

Among these, improved optimization algorithms aim to enhance Gaussian modeling by addressing inherent limitations, such as over-reconstructing certain regions while underrepresenting others. A critical aspect of these improvements is geometry-aware optimization [35, 36, 39], which plays a vital role in accurately reconstructing the underlying 3D structure of objects. A notable work in this direction is 2DGS [35], which employs 2D Gaussian planes to better approximate surface geometry, thereby producing more physically accurate shape representations. These geometric insights have strongly influenced the development of our proposed method.

## 2.2 3D Segmentation in NeRF

NeRF-based 3D segmentation can be categorized into two main approaches:

**Feature Distillation:** Early works such as NVOS [11] and ISRF [48] project 2D features from foundation models into 3D voxel fields. NVOS establishes a cyclic optimization framework that: (1) backprojects 2D features to construct 3D segmentation fields, (2) renders pseudo-masks as prompts for Segment Anything Model (SAM) [49], and (3) iteratively refines the 3D field through reprojection consistency.

**Mask Projection:** Subsequent methods directly leverage 2D masks from foundation models. SA3D [19] uses SAM-generated masks to initialize 3D voxel representations with iterative refinement. MVSeg [12] propagates masks across views using a video tracker. GARField [17] introduces scale-conditioned feature fields to address multi-view inconsistency through geometric-aware mask processing.

The inherent multi-view inconsistency in 2D features makes feature distillation approaches more challenging than mask-based methods. Nonetheless, these works provide valuable insights for 3DGS-based segmentation.

## 2.3 3D Segmentation in Gaussians

Current 3DGS segmentation methods [14, 16, 18, 15, 13] adopt either distillation or contrastive learning frameworks. A common pipeline first extracts 2D features or masks from foundation models (e.g., SAM), then lifts them to 3D Gaussian attributes via learning objectives. During inference, 3D features are reprojected to 2D views for decoding. These approaches differ primarily in how they handle view inconsistency:

**Feature3DGS [14]:** This pioneering work distills SAM features into Gaussian semantic attributes. However, it suffers from a key limitation: direct feature transfer without addressing SAM’s view inconsistency.

**OmniSeg3D [15]:** This contrastive learning-based method clusters inconsistent SAM masks across views. While it achieves better consistency than Feature3DGS using lower-dimensional features, it assumes a single-object representation per Gaussian primitive, limiting its ability to handle complex scenes.

**SAGA [16]:** To address scale inconsistency in SAM masks, SAGA incorporates 3D size awareness during contrastive learning. By constructing scale-disentangled feature spaces, it more effectively resolves multi-view conflicts and enables multi-object representation within Gaussian primitives.

# 3 Method

We propose a novel two-stage framework for 3D segmentation in Gaussian scenes, as illustrated in Fig. 2. Our approach decomposes the challenging 3D segmentation task into two complementary stages that progressively construct accurate instance-level segmentation while ensuring multi-view consistency.

## 3.1 Stage I: Warm-Up Initialization

The continuous rendering capability of 3D Gaussian Splatting allows us to formulate 3D segmentation as a multi-view consistent video segmentation problem. We leverage SAM 2, a state-of-the-art video

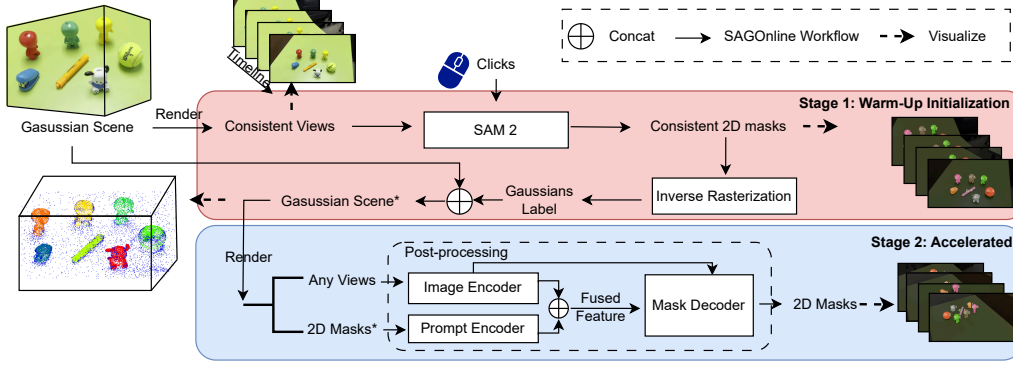


Figure 2: The architecture of SAGOnline. The top part illustrates the Warm-Up Initialization Stage, which first uses SAM 2 to generate consistent segmentation masks across novel views. These 2D masks are then converted into Gaussian labels (i.e., 3D masks) using an inverse rasterization module, resulting in a new Gaussian Scene\*. (Containing instance information.) The bottom part is the Accelerated Stage, which employs a post-processing network to refine the 2D Masks\* and any views rendered from Gaussian Scene\*.

segmentation foundation model, to establish initial segmentation consistency across viewpoints without requiring any task-specific training.

Given a sequence of rendered views  $\{I_t\}_{t=1}^T$  from a pre-trained Gaussian scene  $\mathcal{G}$  (trained by 2DGS [35]), we initialize segmentation prompts on a reference frame and propagate them through adjacent views using SAM 2’s temporal tracking mechanism:

$$\{M_t^{2D}\}_{t=1}^T = \mathcal{F}_{\text{SAM2}}(I_1, \text{prompt}) \rightarrow \{I_t\}_{t=2}^T \quad (1)$$

where  $M_t^{2D} \in \mathbb{N}^{H \times W}$  denotes the 2D instance segmentation masks, with pixel values representing instance IDs ( $H, W$  denote the height and width of the image), and  $\mathcal{F}_{\text{SAM2}}$  represents the video segmentation function of SAM 2.

To aggregate multi-view segmentation masks in 3D space, we propose an *Inverse Projection Voting* scheme that assigns instance labels to Gaussian primitives. For each Gaussian primitive  $G_i \in \mathcal{G}$  with center  $\mathbf{c}_i \in \mathbb{R}^3$ , we project its centroid to all rendered views and collect the corresponding instance IDs from the 2D masks. The final instance label  $l_i$  is assigned to  $G_i$  as follows:

$$l_i = \arg \max_{k \in \mathcal{K}} \sum_{t=1}^T \mathbb{I} [M_t^{2D}(\pi_t(\mathbf{c}_i)) = k] \quad (2)$$

where  $\pi_t : \mathbb{R}^3 \mapsto \mathbb{R}^2$  is the perspective projection operator for view  $t$ .  $\mathcal{K}$  denotes the set of valid instance IDs.  $\mathbb{I}[\cdot]$  is the indicator function.

This voting mechanism accumulates cross-view consensus by selecting the most frequently observed instance ID across all valid projections. The resulting segmented Gaussian representation  $\mathcal{G}_{\text{seg}}$  encodes instance-aware attributes while preserving the original Gaussian properties:

$$\mathcal{G}_{\text{seg}} = \{(G_i, l_i) | G_i \in \mathcal{G}, l_i \in \mathcal{K}\}_{i=1}^N \quad (3)$$

To maximize computational efficiency, we employ a GPU-based parallel computing approach to obtain  $\mathcal{G}_{\text{seg}}$ . For details, please refer to Sec. A.1 in the appendix.

### 3.2 Stage II: Accelerated Segmentation with Arbitrary-view Inference

Building on the warm-up initialization, we propose an accelerated inference framework that removes the adjacency constraint for novel view synthesis, enabling segmentation from arbitrary viewpoints.

Our approach consists of two cascaded components: (1) a Gaussian splatting-based pipeline for efficient generation of novel view renderings and corresponding coarse masks from the segmented 3D Gaussians  $\mathcal{G}_{\text{seg}}$ ; and (2) a lightweight mask refinement network for post-processing the initial segmentation results.

The pre-segmented 3D Gaussian representation enables real-time mask generation through differentiable rendering:

$$M_{\text{coarse}}^{2D} = \mathcal{R}(\mathcal{G}_{\text{seg}}, \theta) \quad (4)$$

where  $\mathcal{R}$  denotes the 3D Gaussian splatting renderer, and  $\theta$  represents the target camera parameters.

To resolve the spatial discontinuity artifacts present in coarse masks, we design a cascaded refinement network  $\mathcal{N}_\phi$  with three key components (visualized in Fig. 2; the detailed structure is provided in Sec. A.2 of the appendix):

- **Image Encoder:** A ResNet-50 backbone (stages 1-4) that extracts multi-scale visual features from the rendered RGB image
- **Prompt Encoder:** A lightweight CNN branch that processes the coarse mask  $M_{\text{coarse}}^{2D}$  to generate segmentation priors
- **Mask Decoder:** A U-Net-style decoder that aggregates features from both encoders via skip connections to produce refined segmentation masks.

The network is supervised using multi-view segmentation labels from Stage I with cross-entropy loss:

$$\mathcal{L}_{\text{refine}} = - \sum_{t=1}^T \sum_{h,w} M_t^{2D}(h,w) \log \hat{M}_t^{2D}(h,w) \quad (5)$$

where  $T$  denotes the number of training views. This design enables efficient mask refinement while maintaining real-time performance (see Section 4.4 for runtime analysis). The prompt-based architecture is inspired by SAM [49], but differs in that it uses rendered coarse masks as automatic prompts rather than manual inputs.

This two-stage approach achieves both efficiency and accuracy in 3D segmentation. Comparative experiments between the two stages are presented in Sec. B.4 of the appendix, demonstrating a 99% similarity in segmentation performance.

## 4 Experiments

### 4.1 Datasets

Our evaluation utilizes two primary datasets: NVOS [11] and the SPIn-NeRF benchmark [12]. The NVOS dataset extends the LLFF dataset [50] by providing instance-level annotations for foreground objects across diverse scenes. The SPIn-NeRF benchmark is a multiview segmentation dataset that offers unified instance segmentation labels across multiple domains. Both datasets are specifically designed for NeRF-based segmentation tasks, ensuring direct compatibility with our methods.

To comprehensively evaluate cross-domain performance, we conduct additional experiments on the Mip-360 [51], LERF-Mask dataset [18], and DesktopObjects-360 [52] scenes. This extended evaluation enables a systematic analysis of our method’s segmentation quality (in both 2D and 3D) and computational efficiency across: 1) indoor/outdoor environments, 2) varying object densities, and 3) different illumination conditions.

### 4.2 Experimental Settings

**Implementation Details:** All experiments are conducted on an NVIDIA RTX 4090 GPU and an i5-11400F CPU, using PyTorch 2.1.0 and CUDA 11.8 within Linux system. All Gaussian scenes used for testing are trained for 30,000 iterations.

Table 1: Instance segmentation results on NVOS and SPIn-NeRF datasets. The metrics employed are mean Intersection over Union (mIoU) and mean Accuracy (mAcc).

Method	NVOS		SPIn-NeRF	
	mIoU (%)	mAcc (%)	mIoU (%)	mAcc (%)
NVOS [11]	70.1	92.0	-	-
ISRF [48]	83.8	96.4	-	-
MVSeg [12]	-	-	91.0	98.9
SA3D [19]	90.3	98.2	92.4	98.9
OmniSeg3D [15]	91.7	98.4	<b>95.2</b>	99.2
SA3D-GS [53]	92.2	98.5	93.2	99.1
SAGA [16]	92.6	98.6	93.4	99.2
Click-Gaussian [13]	-	-	94.0	-
<b>SAGOnline (Ours)</b>	<b>92.7</b>	<b>98.7</b>	<b>95.2</b>	<b>99.3</b>

### 4.3 Quantitative Segmentation Performance

We evaluate our method on two challenging benchmarks: the NVOS dataset and the SPIn-NeRF dataset, comparing it against various approaches including NVOS [11], ISRF [48], MVSeg [12], SA3D [19], OmniSeg3D [15], SA3D-GS [53], SAGA [16], and Click-Gaussian [13]. Notably, OmniSeg3D is the previous top performer on SPIn-NeRF, while SAGA holds the leading position on NVOS.

As shown in Table 1, our method achieves new state-of-the-art performance on the NVOS dataset, surpassing all competitors by narrow yet consistent margins. Specifically, SAGOnline attains 92.7% mIoU and 98.7% mAcc, outperforming SAGA (the previous SOTA) by 0.1% in both metrics.

On the SPIn-NeRF dataset, our proposed **SAGOnline** also achieves state-of-the-art results, with 95.2% mIoU and 99.3% mAcc, demonstrating notable improvements over existing methods. Notably, while our method matches the mIoU of OmniSeg3D (the previous best), it surpasses its mAcc by 0.1%, indicating superior consistency in segmentation quality.

As illustrated in Fig. 3, our algorithm demonstrates robust segmentation performance across diverse environments and object categories. The Fork scenario, in particular, highlights our method’s ability to capture fine structural details that are missing from the ground truth annotations.

Since SA3D, OmniSeg3D, SAGA, Click-Gaussian, and MVSeg all rely on the same foundational image model, namely SAM, these algorithms exhibit similar segmentation performance. The key differences among these methods lie in how effectively they utilize SAM for information extraction and how well they address its limitations in generating consistent and coherent masks. While these methods enable zero-shot segmentation, this also imposes an upper bound on potential accuracy improvements.

Like these approaches, our method adopts SAM 2, and thus our performance similarly depends on the underlying image model, leading to comparable segmentation results. However, the marginal yet consistent improvements over strong baselines suggest that our technical innovations—particularly in the transformation of segmentation tasks—enable more effective use of large-scale image models, thereby better exploiting their full capabilities.

### 4.4 Time Efficiency

The temporal efficiency of 3D segmentation algorithms critically impacts their practical deployment, particularly in latency-sensitive applications such as AR/VR systems and interactive 3D scene annotation. We conduct comprehensive time comparisons between our SAGOnline and existing approaches under identical multi-object scene, with quantitative results summarized in Table 2.

Our proposed SAGOnline framework demonstrates significant improvements in both training efficiency and inference speed compared to existing approaches, as shown in Table 2. Specifically, SAGOnline achieves **zero training time**, matching SA3D’s online learning capability while outperforming offline methods such as GARField (45min) and Feature3DGS (35min). This eliminates the

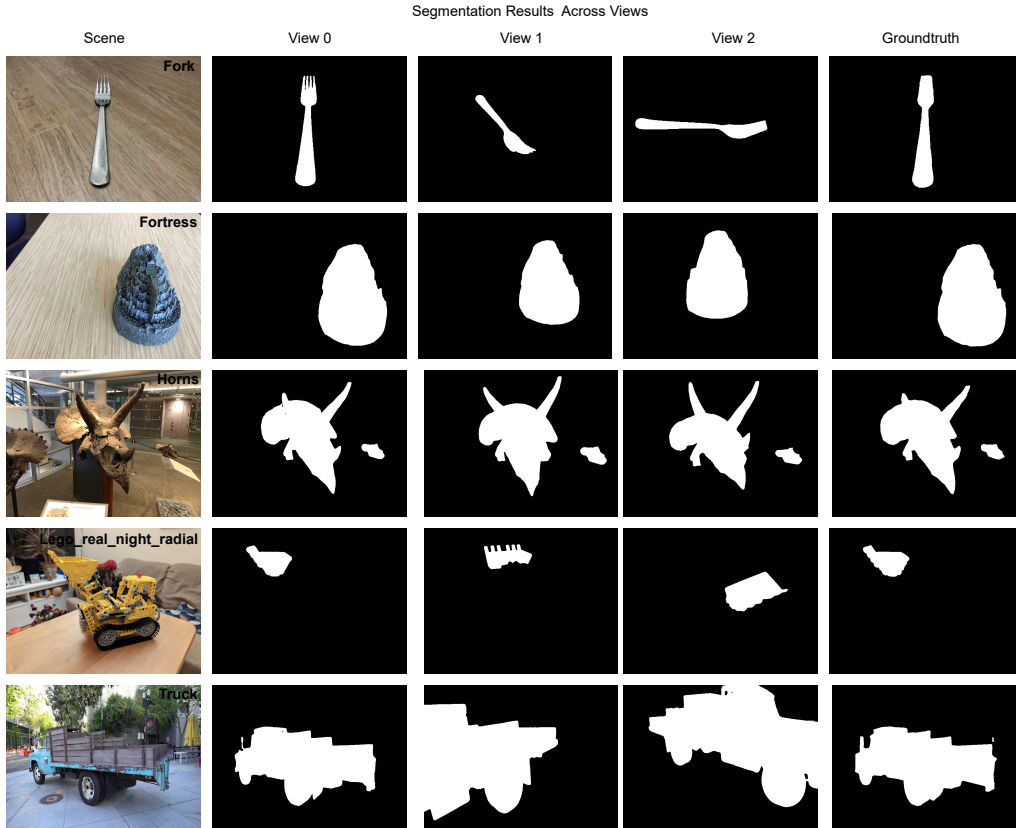


Figure 3: Qualitative segmentation results of our method. The first col shows representative scenarios from different datasets. 2nd - 4th cols display our segmentation outputs. 5th col shows the ground truth for view 0. Notably, in the Fork scenario (first row), our method captures finer geometric details than those found in the ground truth annotations.

Table 2: Time Efficiency Comparison on Multi-object Scene.

Method	Training	Inference
SA3D	0	>50 s
GARField	45 min	3 s
Feature3DGS	35 min	510 ms
OmniSeg3D	37 min	463 ms
SAGA	32 min	31 ms
SAGOnline (Warmup)	0	97 ms
SAGOnline (Accelerated)	-	<b>27 ms</b>

preprocessing bottleneck commonly found in distillation and contrastive learning approaches. Regarding inference speed, the accelerated stage of SAGOnline achieves a remarkable **27 ms per frame** (37 FPS), representing a 13% improvement over SAGA (31ms) and is **17× faster** than OmniSeg3D (463ms).

This performance breakthrough is enabled by: (1) an efficient GPU-accelerated algorithm that directly extracts instance information for each Gaussian primitive from 2D masks; and (2) leveraging large video models to process Gaussian representations directly, thereby achieving cost-free algorithm initialization.

The two-stage execution framework intelligently balances accuracy and speed. The first warm-up stage (97ms) builds scene priors while generating consistent segmentation masks for novel views.

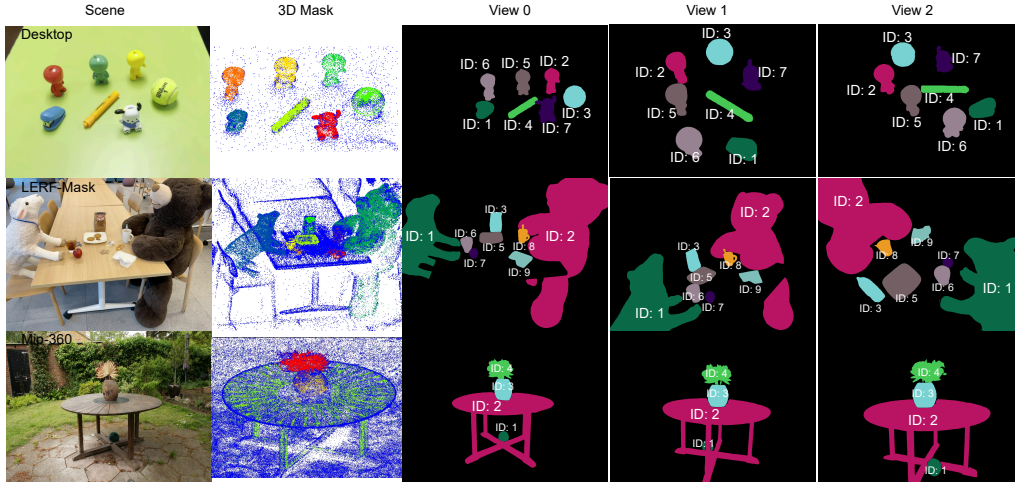


Figure 4: Multi-object segmentation comparison. The 1st col shows representative scenarios from different datasets. The 2nd col shows the 3D mask of the primitive mean value points. The 3rd - 5th cols present our segmentation outputs. Different color represent different objects.

The accelerated stage (27ms) achieves real-time performance through dynamic rendering. Notably, the inference speed in the accelerated stage is significantly faster than that of the warm-up stage. Therefore, the transition time between the two stages must be considered. We measure both the time required to generate 3D masks from 2D masks and the refinement time of the post-processing network. Specifically:

- **2D-to-3D mask generation:** 1466 ms (1.47 seconds)
- **Post-network refinement:** 4 minutes 36 seconds

This results in a total transition time of approximately **five minutes** between the two stages. For more experiments on the impact of 2D masks on 3D mask quality, please refer to Sec. B.3 in the appendix.

These results demonstrate SAGOnline’s strong potential for latency-critical applications, establishing a new state-of-the-art in online 3D scene understanding while maintaining competitive segmentation accuracy.

#### 4.5 Multi Objects Segmentation & Tracking

While current benchmarks like NVOS and Spin-NeRF provide valuable evaluation platforms, they exhibit two limitations: (1) scenes contain only one primary object of interest; (2) evaluation relies on 2D metric aggregation, which may not fully reflect 3D segmentation quality. To further evaluate our method, we conduct additional experiments on Mip-360, LERF-Mask, and DesktopObjects-360 datasets.

Fig. 4 demonstrates the multi-object segmentation results of our algorithm across different datasets. As shown in the second column, our method accurately segments each object instance from a 3D perspective in multi-object scenes. The third to fifth columns illustrate that the segmentation remains precise across different viewpoints while maintaining consistent object IDs, indicating successful multi-view consistent segmentation and tracking - a capability lacking in existing approaches.

This robust performance stems from our algorithm’s first-stage generation of global 3D masks, which provide complete 3D coordinates for each object instance. Consequently, our method achieves accurate object localization regardless of viewpoint changes or occlusions. Additional qualitative results are shown in Sec. B.2 in the appendix.



Figure 5: Comparison of Post-Processing Effects. The left shows the segmentation result obtained directly from the mask rendered by Gaussian scene\* without post-processing. The right shows the refined 2D mask and the improved segmentation result after post-processing.

#### 4.6 Ablation Experiments

The post-processing algorithm is designed to refine the rendered segmentation masks to more precise results. We conduct ablation studies to validate its effectiveness. As shown in Fig. 5, the rendered masks produce discrete scattered points, while our post-processing algorithm effectively transforms these sparse points into continuous segmentation masks.

### 5 Conclusion

We present SAGOnline, a lightweight, zero-shot framework for real-time, multi-view consistent 3D segmentation in Gaussian scenes. By extending SAM 2 to 3D without requiring additional training, our method enables interactive segmentation from sparse user clicks while preserving rendering quality. Leveraging an efficient 2D mask processing algorithm, SAGOnline rapidly generates accurate 3D masks, achieving inference speeds that surpass existing methods. Key advantages include: (1) **Efficiency**—the fastest segmentation inference speed to date (27 ms/frame), outperforming prior work; (2) **Convenience**—no additional pre-training required, enabling immediate deployment; and (3) **Accuracy**—state-of-the-art segmentation performance on the NVOS and Spin-Nerf benchmarks. Our framework supports practical AR/VR applications, and future work will explore extending current 3D segmentation algorithms from static to dynamic scenes.

### References

- [1] Ben Mildenhall, Pratul P. Srinivasan, Matthew Tancik, Jonathan T. Barron, Ravi Ramamoorthi, and Ren Ng. NeRF: representing scenes as neural radiance fields for view synthesis. *Communications of the ACM*, 65(1):99–106, December 2021.
- [2] Bernhard Kerbl, Georgios Kopanas, Thomas Leimkühler, and George Drettakis. 3D gaussian splatting for real-time radiance field rendering. *ACM Transactions on Graphics*, 42(4):139–1, 2023.
- [3] Yanqi Bao, Tianyu Ding, Jing Huo, Yaoli Liu, Yuxin Li, Wenbin Li, Yang Gao, and Jiebo Luo. 3D gaussian splatting: Survey, technologies, challenges, and opportunities. *IEEE Transactions on Circuits and Systems for Video Technology*, pages 1–1, 2025.
- [4] Quentin Herau, Moussab Bennehar, Arthur Moreau, Nathan Piasco, Luis Roldão, Dzmitry Tsishkou, Cyrille Migniot, Pascal Vasseur, and Cédric Démonceaux. 3DGS-Calib: 3d gaussian splatting for multimodal spatiotemporal calibration. In *2024 IEEE/RSJ International Conference on Intelligent Robots and Systems (IROS)*, pages 8315–8321, 2024.
- [5] Ziyi Yang, Xinyu Gao, Wen Zhou, Shaohui Jiao, Yuqing Zhang, and Xiaogang Jin. Deformable 3d gaussians for high-fidelity monocular dynamic scene reconstruction. In *Proceedings of the IEEE/CVF Conference on Computer Vision and Pattern Recognition (CVPR)*, pages 20331–20341, 2024.
- [6] Chi Yan, Delin Qu, Dan Xu, Bin Zhao, Zhigang Wang, Dong Wang, and Xuelong Li. GS-SLAM: Dense visual slam with 3d gaussian splatting. In *Proceedings of the IEEE/CVF Conference on Computer Vision and Pattern Recognition (CVPR)*, pages 19595–19604, 2024.
- [7] Hongjia Zhai, Gan Huang, Qirui Hu, Guanglin Li, Hujun Bao, and Guofeng Zhang. NIS-SLAM: Neural implicit semantic rgb-d slam for 3d consistent scene understanding. *IEEE Transactions on Visualization and Computer Graphics*, 30(11):7129–7139, 2024.

- [8] Nikhil Keetha, Jay Karhade, Krishna Murthy Jatavallabhula, Gengshan Yang, Sebastian Scherer, Deva Ramanan, and Jonathon Luiten. SplaTAM: Splat, track & map 3d gaussians for dense rgb-d slam. In *Proceedings of the IEEE/CVF Conference on Computer Vision and Pattern Recognition (CVPR)*, pages 21357–21366, 2024.
- [9] Xiaoyu Zhou, Zhiwei Lin, Xiaojun Shan, Yongtao Wang, Deqing Sun, and Ming-Hsuan Yang. Drivinggaussian: Composite gaussian splatting for surrounding dynamic autonomous driving scenes. In *Proceedings of the IEEE/CVF Conference on Computer Vision and Pattern Recognition (CVPR)*, pages 21634–21643, 2024.
- [10] Renxiang Xiao, Wei Liu, Yushuai Chen, and Liang Hu. LiV-GS: Lidar-vision integration for 3d gaussian splatting slam in outdoor environments. *IEEE Robotics and Automation Letters*, 10(1):421–428, 2025.
- [11] Zhongzheng Ren, Aseem Agarwala, Bryan Russell, Alexander G. Schwing, and Oliver Wang. Neural volumetric object selection. In *Proceedings of the IEEE/CVF Conference on Computer Vision and Pattern Recognition (CVPR)*, pages 6123–6132, 2022.
- [12] Ashkan Mirzaei, Tristan Aumentado-Armstrong, Konstantinos G. Derpanis, Jonathan Kelly, Marcus A. Brubaker, Igor Gilitschenski, and Alex Levinshtein. SPIn-NeRF: Multiview segmentation and perceptual inpainting with neural radiance fields. In *Proceedings of the IEEE/CVF Conference on Computer Vision and Pattern Recognition (CVPR)*, pages 20669–20679, 2023.
- [13] Seokhun Choi, Hyeonseop Song, Jaechul Kim, Taehyeong Kim, and Hoseok Do. Click-Gaussian: Interactive segmentation to any 3D gaussians. In *Proceedings of the European Conference on Computer Vision (ECCV)*, page 289–305, 2024.
- [14] Shijie Zhou, Haoran Chang, Sicheng Jiang, Zhiwen Fan, Zehao Zhu, Dejjia Xu, Pradyumna Chari, Suyu You, Zhangyang Wang, and Achuta Kadambi. Feature 3DGS: Supercharging 3D gaussian splatting to enable distilled feature fields. In *Proceedings of the IEEE/CVF Conference on Computer Vision and Pattern Recognition (CVPR)*, pages 21676–21685, 2024.
- [15] Haiyang Ying, Yixuan Yin, Jinzhi Zhang, Fan Wang, Tao Yu, Ruqi Huang, and Lu Fang. OmniSeg3D: Omniversal 3D segmentation via hierarchical contrastive learning. In *Proceedings of the IEEE/CVF Conference on Computer Vision and Pattern Recognition (CVPR)*, pages 20612–20622, 2024.
- [16] Jiazhong Cen, Jiemin Fang, Chen Yang, Lingxi Xie, Xiaopeng Zhang, Wei Shen, and Qi Tian. Segment any 3d gaussians. *Proceedings of the AAAI Conference on Artificial Intelligence*, 39(2):1971–1979, Apr. 2025.
- [17] Chung Min Kim, Mingxuan Wu, Justin Kerr, Ken Goldberg, Matthew Tancik, and Angjoo Kanazawa. GARField: Group anything with radiance fields. In *Proceedings of the IEEE/CVF Conference on Computer Vision and Pattern Recognition (CVPR)*, pages 21530–21539, 2024.
- [18] Mingqiao Ye, Martin Danelljan, Fisher Yu, and Lei Ke. Gaussian Grouping: Segment and edit anything in 3D scenes. In *Proceedings of the European Conference on Computer Vision (ECCV)*, pages 162–179, 2025.
- [19] Jiazhong Cen, Zanwei Zhou, Jiemin Fang, chen yang, Wei Shen, Lingxi Xie, Dongsheng Jiang, XIAOPENG ZHANG, and Qi Tian. Segment anything in 3D with NeRFs. In *Advances in Neural Information Processing Systems*, volume 36, pages 25971–25990, 2023.
- [20] Umangi Jain, Ashkan Mirzaei, and Igor Gilitschenski. Gaussiancut: Interactive segmentation via graph cut for 3d gaussian splatting. In A. Globerson, L. Mackey, D. Belgrave, A. Fan, U. Paquet, J. Tomczak, and C. Zhang, editors, *Advances in Neural Information Processing Systems*, volume 37, pages 89184–89212. Curran Associates, Inc., 2024. URL [https://proceedings.neurips.cc/paper\\_files/paper/2024/file/a26f3dc32a913b77fa70c33ffa5dcb37-Paper-Conference.pdf](https://proceedings.neurips.cc/paper_files/paper/2024/file/a26f3dc32a913b77fa70c33ffa5dcb37-Paper-Conference.pdf).
- [21] QiuHong Shen, Xingyi Yang, and Xinchao Wang. Flashsplat: 2d to 3d gaussian splatting segmentation solved optimally. In *Computer Vision – ECCV 2024: 18th European Conference, Milan, Italy, September 29 – October 4, 2024, Proceedings, Part XXII*, page 456–472, Berlin, Heidelberg, 2024. Springer-Verlag. ISBN 978-3-031-72669-9. doi: 10.1007/978-3-031-72670-5\_26. URL [https://doi.org/10.1007/978-3-031-72670-5\\_26](https://doi.org/10.1007/978-3-031-72670-5_26).
- [22] Nikhila Ravi, Valentin Gabeur, Yuan-Ting Hu, Ronghang Hu, Chaitanya Ryali, Tengyu Ma, Haitham Khedr, Roman Rädle, Chloe Rolland, Laura Gustafson, Eric Mintun, Junting Pan, Kalyan Vasudev Alwala, Nicolas Carion, Chao-Yuan Wu, Ross Girshick, Piotr Dollár, and Christoph Feichtenhofer. SAM 2: Segment anything in images and videos. *arXiv preprint arXiv:2408.00714*, 2024.

- [23] Chen Yang, Sikuang Li, Jiemin Fang, Ruofan Liang, Lingxi Xie, Xiaopeng Zhang, Wei Shen, and Qi Tian. Gaussianobject: High-quality 3D object reconstruction from four views with gaussian splatting. *ACM Transactions on Graphics*, 43(6), November 2024.
- [24] Yuedong Chen, Haofei Xu, Chuanxia Zheng, Bohan Zhuang, Marc Pollefeys, Andreas Geiger, Tat-Jen Cham, and Jianfei Cai. MVSplat: Efficient 3d gaussian splatting from sparse multi-view images. In *Proceedings of the European Conference on Computer Vision (ECCV)*, pages 370–386, 2025.
- [25] Jiahe Li, Jiawei Zhang, Xiao Bai, Jin Zheng, Xin Ning, Jun Zhou, and Lin Gu. Dngaussian: Optimizing sparse-view 3d gaussian radiance fields with global-local depth normalization. In *2024 IEEE/CVF Conference on Computer Vision and Pattern Recognition (CVPR)*, pages 20775–20785, 2024.
- [26] Zehao Zhu, Zhiwen Fan, Yifan Jiang, and Zhangyang Wang. Fsgs: Real-time few-shot view synthesis using gaussian splatting. In *Computer Vision – ECCV 2024*, pages 145–163, Cham, 2025.
- [27] David Charatan, Sizhe Lester Li, Andrea Tagliasacchi, and Vincent Sitzmann. Pixelsplat: 3d gaussian splats from image pairs for scalable generalizable 3d reconstruction. In *2024 IEEE/CVF Conference on Computer Vision and Pattern Recognition (CVPR)*, pages 19457–19467, 2024.
- [28] Joo Chan Lee, Daniel Rho, Xiangyu Sun, Jong Hwan Ko, and Eunbyung Park. Compact 3D gaussian representation for radiance field. In *Proceedings of the IEEE/CVF Conference on Computer Vision and Pattern Recognition (CVPR)*, pages 21719–21728, 2024.
- [29] Simon Niedermayr, Josef Stumpfegger, and Rüdiger Westermann. Compressed 3d gaussian splatting for accelerated novel view synthesis. In *2024 IEEE/CVF Conference on Computer Vision and Pattern Recognition (CVPR)*, pages 10349–10358, 2024.
- [30] Xinjie Zhang, Xingtong Ge, Tongda Xu, Dailan He, Yan Wang, Hongwei Qin, Guo Lu, Jing Geng, and Jun Zhang. Gaussianimage: 1000 fps image representation and compression by 2d gaussian splatting. In *Computer Vision – ECCV 2024*, pages 327–345, Cham, 2025.
- [31] Yingwenqi Jiang, Jiadong Tu, Yuan Liu, Xifeng Gao, Xiaoxiao Long, Wenping Wang, and Yuexin Ma. Gaussianshader: 3d gaussian splatting with shading functions for reflective surfaces. In *2024 IEEE/CVF Conference on Computer Vision and Pattern Recognition (CVPR)*, pages 5322–5332, 2024.
- [32] Luis Bolanos, Shih-Yang Su, and Helge Rhodin. Gaussian shadow casting for neural characters. In *2024 IEEE/CVF Conference on Computer Vision and Pattern Recognition (CVPR)*, pages 20997–21006, 2024.
- [33] Zehao Yu, Anpei Chen, Binbin Huang, Torsten Sattler, and Andreas Geiger. Mip-splatting: Alias-free 3d gaussian splatting. In *2024 IEEE/CVF Conference on Computer Vision and Pattern Recognition (CVPR)*, pages 19447–19456, 2024.
- [34] Zhiwen Yan, Weng Fei Low, Yu Chen, and Gim Hee Lee. Multi-scale 3d gaussian splatting for anti-aliased rendering. In *2024 IEEE/CVF Conference on Computer Vision and Pattern Recognition (CVPR)*, pages 20923–20931, 2024.
- [35] Binbin Huang, Zehao Yu, Anpei Chen, Andreas Geiger, and Shenghua Gao. 2D gaussian splatting for geometrically accurate radiance fields. In *ACM SIGGRAPH 2024 Conference Papers*, 2024.
- [36] Antoine Guédon and Vincent Lepetit. SuGaR: Surface-aligned gaussian splatting for efficient 3D mesh reconstruction and high-quality mesh rendering. In *Proceedings of the IEEE/CVF Conference on Computer Vision and Pattern Recognition (CVPR)*, pages 5354–5363, 2024.
- [37] Yang Fu, Xiaolong Wang, Sifei Liu, Amey Kulkarni, Jan Kautz, and Alexei A. Efros. COLMAP-free 3d gaussian splatting. In *Proceedings of the IEEE/CVF Conference on Computer Vision and Pattern Recognition (CVPR)*, pages 20796–20805, 2024.
- [38] Jiahui Zhang, Fangneng Zhan, Muyu Xu, Shijian Lu, and Eric Xing. Fregs: 3d gaussian splatting with progressive frequency regularization. In *2024 IEEE/CVF Conference on Computer Vision and Pattern Recognition (CVPR)*, pages 21424–21433, 2024.
- [39] Tao Lu, Mulin Yu, Linning Xu, Yuanbo Xiangli, Limin Wang, Dahua Lin, and Bo Dai. Scaffold-gs: Structured 3d gaussians for view-adaptive rendering. In *2024 IEEE/CVF Conference on Computer Vision and Pattern Recognition (CVPR)*, pages 20654–20664, 2024.
- [40] Jin-Chuan Shi, Miao Wang, Hao-Bin Duan, and Shao-Hua Guan. Language embedded 3d gaussians for open-vocabulary scene understanding. In *2024 IEEE/CVF Conference on Computer Vision and Pattern Recognition (CVPR)*, pages 5333–5343, 2024.

- [41] Minghan Qin, Wanhua Li, Jiawei Zhou, Haoqian Wang, and Hanspeter Pfister. Langsplat: 3d language gaussian splatting. In *2024 IEEE/CVF Conference on Computer Vision and Pattern Recognition (CVPR)*, pages 20051–20060, 2024.
- [42] Guanjun Wu, Taoran Yi, Jiemin Fang, Lingxi Xie, Xiaopeng Zhang, Wei Wei, Wenyu Liu, Qi Tian, and Xinggang Wang. 4d gaussian splatting for real-time dynamic scene rendering. In *2024 IEEE/CVF Conference on Computer Vision and Pattern Recognition (CVPR)*, pages 20310–20320, 2024.
- [43] Ziyi Yang, Xinyu Gao, Wen Zhou, Shaohui Jiao, Yuqing Zhang, and Xiaogang Jin. Deformable 3d gaussians for high-fidelity monocular dynamic scene reconstruction. In *2024 IEEE/CVF Conference on Computer Vision and Pattern Recognition (CVPR)*, pages 20331–20341, 2024.
- [44] Yuelang Xu, Bengwang Chen, Zhe Li, Hongwen Zhang, Lizhen Wang, Zerong Zheng, and Yebin Liu. Gaussian head avatar: Ultra high-fidelity head avatar via dynamic gaussians. In *2024 IEEE/CVF Conference on Computer Vision and Pattern Recognition (CVPR)*, pages 1931–1941, 2024.
- [45] Jorge Condor, Sebastien Speierer, Lukas Bode, Aljaz Bozic, Simon Green, Piotr Didyk, and Adrian Jarabo. Don’t splat your gaussians: Volumetric ray-traced primitives for modeling and rendering scattering and emissive media. *ACM Trans. Graph.*, 44(1), February 2025.
- [46] Nicolas Moenne-Loccoz, Ashkan Mirzaei, Or Perel, Riccardo de Lutio, Janick Martinez Esturo, Gavriel State, Sanja Fidler, Nicholas Sharp, and Zan Gojcic. 3d gaussian ray tracing: Fast tracing of particle scenes. *ACM Trans. Graph.*, 43(6), November 2024.
- [47] Guikun Chen and Wenguan Wang. A survey on 3d gaussian splatting. *arXiv preprint arXiv:2401.03890*, 2025.
- [48] Rahul Goel, Dhawal Sirikonda, Saurabh Saini, and P J Narayanan. Interactive segmentation of radiance fields. In *Proceedings of the IEEE/CVF Conference on Computer Vision and Pattern Recognition (CVPR)*, pages 4201–4211, 2023.
- [49] Alexander Kirillov, Eric Mintun, Nikhila Ravi, Hanzi Mao, Chloe Rolland, Laura Gustafson, Tete Xiao, Spencer Whitehead, Alexander C. Berg, Wan-Yen Lo, Piotr Dollar, and Ross Girshick. Segment anything. In *Proceedings of the IEEE/CVF International Conference on Computer Vision (ICCV)*, pages 4015–4026, October 2023.
- [50] Ben Mildenhall, Pratul P. Srinivasan, Rodrigo Ortiz-Cayon, Nima Khademi Kalantari, Ravi Ramamoorthi, Ren Ng, and Abhishek Kar. Local light field fusion: practical view synthesis with prescriptive sampling guidelines. *ACM Transactions on Graphics*, 38(4), July 2019.
- [51] Jonathan T. Barron, Ben Mildenhall, Dor Verbin, Pratul P. Srinivasan, and Peter Hedman. Mip-NeRF 360: Unbounded anti-aliased neural radiance fields. In *Proceedings of the IEEE/CVF Conference on Computer Vision and Pattern Recognition (CVPR)*, pages 5460–5469, 2022.
- [52] Wentao Sun, Hanqing Xu, Quanyun Wu, Dedong Zhang, Yiping Chen, Lingfei Ma, John S. Zelek, and Jonathan Li. Pointgauss: Point cloud-guided multi-object segmentation for gaussian splatting, 2025. URL <https://arxiv.org/abs/2508.00259>.
- [53] Jiazhong Cen, Jiemin Fang, Zanwei Zhou, Chen Yang, Lingxi Xie, Xiaopeng Zhang, Wei Shen, and Qi Tian. Segment anything in 3d with radiance fields. *arXiv preprint arXiv:2304.12308*, 2024.

# Technical Appendices and Supplementary Material

## A Method

### A.1 Instance Label Aggregation

To quickly generate 3D masks from 2D masks, we designed an algorithm based on voting and projection. The pseudocode is shown in Alg. 1. This algorithm performs instance segmentation for Gaussian primitives by aggregating multi-view 2D instance predictions into consistent 3D labels through a voting scheme: for each rendered viewpoint, it collects pixel-level instance votes for visible Gaussian primitives, accumulates these votes in a histogram across all views, and assigns each Gaussian the instance label with the highest vote count. This approach effectively resolves view-dependent ambiguities while maintaining computational efficiency through GPU-optimized tensor operations and sparse indexing.

### A.2 Post-processing

The post-processing network employs a dual-branch encoder-decoder architecture with multi-scale feature fusion. It processes 3-channel input images and 1-channel coarse masks of size  $H \times W$ . The structure is illustrated in Fig. 6.

**Image Encoder:** This branch uses a ResNet50 backbone: 1) A stem block (Conv + BN + ReLU) reduces the spatial resolution to  $H/2 \times W/2$  with 64 channels. 2) Four residual layers (Layer1–4) progressively extract features (e1–e4) at  $1/4$ ,  $1/8$ ,  $1/16$ , and  $1/32$  resolutions, with 256, 512, 1024, and 2048 channels, respectively.

**Prompt Encoder:** This branch consists of three ConvBlocks with max pooling, generating multi-scale features at  $1/2$ ,  $1/4$ , and  $1/8$  resolutions, with 32, 64, and 128 channels, respectively.

**Feature Fusion:** Prompt Encoder features are upsampled to a  $1/32$  resolution (128 channels) and concatenated with e4. A  $1 \times 1$  convolution followed by BN, ReLU, and Channel Attention (CA) compresses the fused features to 512 channels.

**Mask Decoder:** The decoder follows a U-Net structure. Specifically, it progressively upsamples features through three stages: 1) Each stage applies a transposed convolution for  $2 \times$  upsampling; 2) The corresponding encoder feature (e3/e2/e1) undergoes CA before concatenation; 3) Two convolutional layers with CA refine the merged features. A final  $4 \times$  upsampling step produces a 2-channel output with sigmoid activation.

## B Experiments

### B.1 Experiments Settings

SAGOnline requires an initial prompt to specify the object of interest. We initialize this by randomly clicking on the ground truth object, with no additional prompts required during inference. All experiments were conducted using the same hardware configuration. For the Spin-NeRF dataset, we treat the training image sequence—sorted lexicographically by filename—as a pseudo-temporal sequence for algorithm initialization. Similarly, for the NVOS dataset, we establish the pseudo-temporal sequence through filename-based sorting and provide the initial target location via random clicks on the ground truth object.

### B.2 Qualitative Evaluation

A key advantage of our method is its capability for simultaneous multi-object segmentation and tracking while generating global 3D masks. Fig. 7 presents additional experimental results on multi-object segmentation.

---

**Algorithm 1** Instance Label Aggregation
 

---

**Require:**  $\mathcal{C}$ : Set of camera viewpoints

- 1:  $\mathcal{G}$ : Gaussian splatting model
- 2:  $\mathcal{M} = \{\mathbf{M}_1, \dots, \mathbf{M}_N\}$ : Precomputed instance masks
- 3:  $H \times W$ : Rendering resolution

**Ensure:** Instance labels  $\mathbf{L} \in \mathbb{Z}^{|\mathcal{G}|}$ 

- 4: Initialize count matrix  $\mathbf{C} \leftarrow \mathbf{0}^{|\mathcal{G}| \times K}$   $\triangleright K$ : max instance ID
  - 5: **for** each viewpoint  $\mathbf{C}_i \in \mathcal{C}$  **do**
  - 6:   Render frame:  $\mathbf{R}_i \leftarrow \text{Render}(\mathbf{C}_i, \mathcal{G})$
  - 7:   Extract index map  $\mathbf{I}_i \leftarrow \text{Flatten}(\mathbf{R}_i.\text{idx\_image}) \in \mathbb{Z}^{HW}$
  - 8:   Get instance mask  $\mathbf{M}_i \leftarrow \text{Flatten}(\mathcal{M}[i]) \in \{0, 1\}^{HW}$
  - 9:   Compute valid pixel mask:  $\mathbf{V} \leftarrow (\mathbf{I}_i \geq 0)$
  - 10:   Filter valid entries:  $\hat{\mathbf{I}}_i \leftarrow \mathbf{I}_i[\mathbf{V}]$ ,  $\hat{\mathbf{M}}_i \leftarrow \mathbf{M}_i[\mathbf{V}]$
  - 11:   **if**  $\|\hat{\mathbf{I}}_i\| > 0$  **then**
  - 12:     Find unique pairs:  $\{(\mathbf{p}_k, \mathbf{m}_k)\} \leftarrow \text{Unique}(\hat{\mathbf{I}}_i, \hat{\mathbf{M}}_i)$
  - 13:     Count occurrences:  $\mathbf{c}_k \leftarrow \text{Histogram}(\hat{\mathbf{I}}_i, \hat{\mathbf{M}}_i)$
  - 14:     Update count matrix:  $\mathbf{C}[\mathbf{p}_k, \mathbf{m}_k] += \mathbf{c}_k$
  - 15:   **end if**
  - 16: **end for**
  - 17: Determine final labels:  $\mathbf{L} \leftarrow \underset{k}{\text{argmax}} \mathbf{C}[:, k]$
  - 18: **return**  $\mathbf{L}$
- 

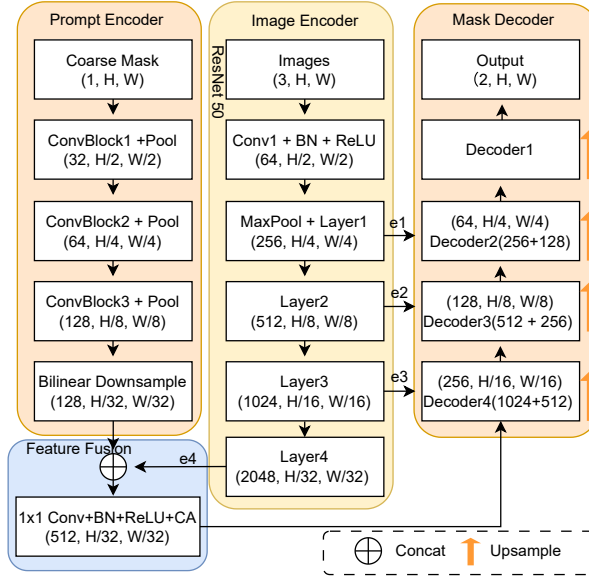


Figure 6: Post-processing architecture. It has three parts: Prompt Encoder, Image Encoder, and a Mask Decoder.

### B.3 Robustness Analysis

Since our algorithm generates 3D masks from 2D segmentation results, we conducted experiments to investigate the relationship between 3D mask quality and the number of available 2D masks. Specifically, we randomly selected varying numbers of 2D masks as input for generating 3D masks. By gradually increasing the number of input masks, we observed changes in the quality of the resulting 3D masks and recorded the corresponding generation times. This analysis offers insights into the robustness and scalability of our 3D reconstruction process.

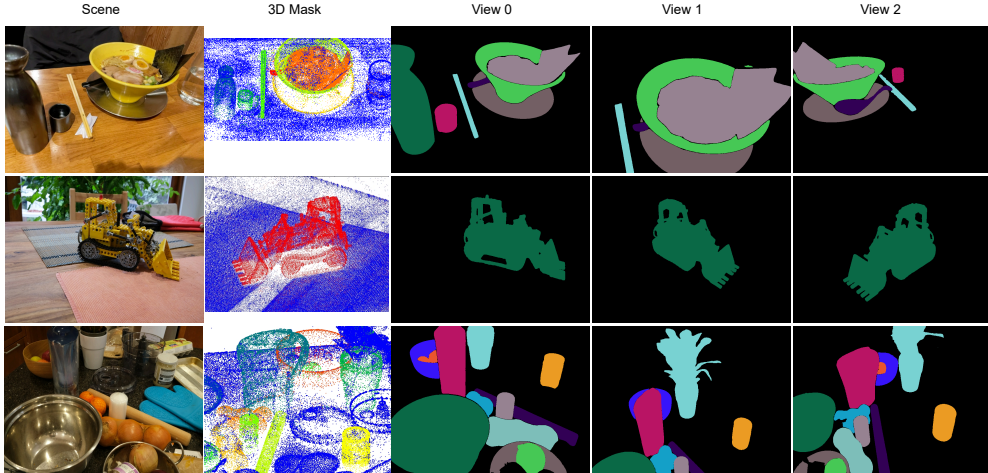


Figure 7: Multi-object segmentation comparison. The 1st col shows representative scenarios from different datasets. The 2nd col shows the 3D mask of primitive mean value points. The 3rd - 5th cols present our segmentation outputs, where different colors indicate different object instances.

Table 3: Time consumption of 3D mask generation with different numbers of 2D masks.

Number of 2D masks	Time (ms)
Full (206)	1466
100	571
50	384
25	224
12	162
6	140
3	114
1	111

As shown in Fig. 8, as the number of input 2D masks increases, more Gaussian primitives are assigned instance ID information. However, even with as few as six 2D masks, the generated 3D masks can still clearly distinguish different object instances. This demonstrates the strong robustness of our algorithm, which can produce relatively accurate global 3D masks using only a small number of 2D inputs.

Table 3 shows the time consumption for generating 3D masks with varying numbers of 2D masks. As shown, the time required to generate the 3D mask decreases as the number of 2D masks processed reduces, from 1466 ms for 206 2D masks to 111 ms for a single 2D mask. Overall, our algorithm generates masks quickly, meeting real-time performance requirements.

#### B.4 Stage 2: Accelerated Stage

To further investigate the difference in segmentation accuracy between the accelerated and warm-up stages, we compared the segmentation results of the two stages in multiple instance segmentation experiments. The experimental results are shown in Fig. 9. As seen in the figure, the segmentation results from both stages are consistent, with no significant differences observed.

Additionally, we assumed that the results obtained from Stage 1 represented the ground truth. We then calculated the accuracy of the segmentation results from Stage 2 in comparison to those from Stage 1. The experiments showed that the overall accuracy reached 99.89%, and the mean Intersection over Union (mIoU) reached 98.47%. These results demonstrate that the two stages have equivalent segmentation capabilities. This is because Stage 2 leverages the information obtained from Stage 1

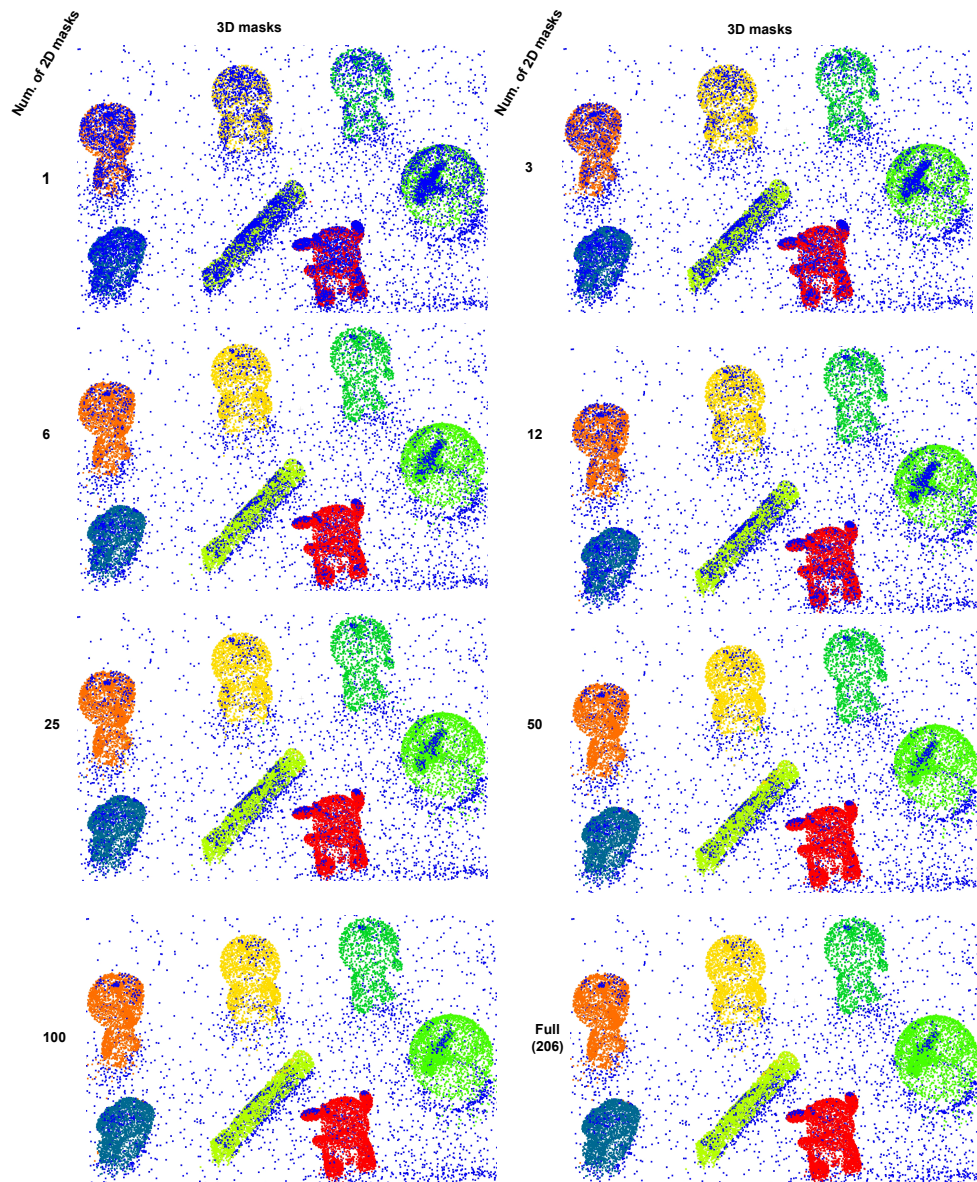


Figure 8: 3D masks with different number of 2D masks. It illustrates the rendering effects of 3D masks generated from different numbers of input 2D masks.

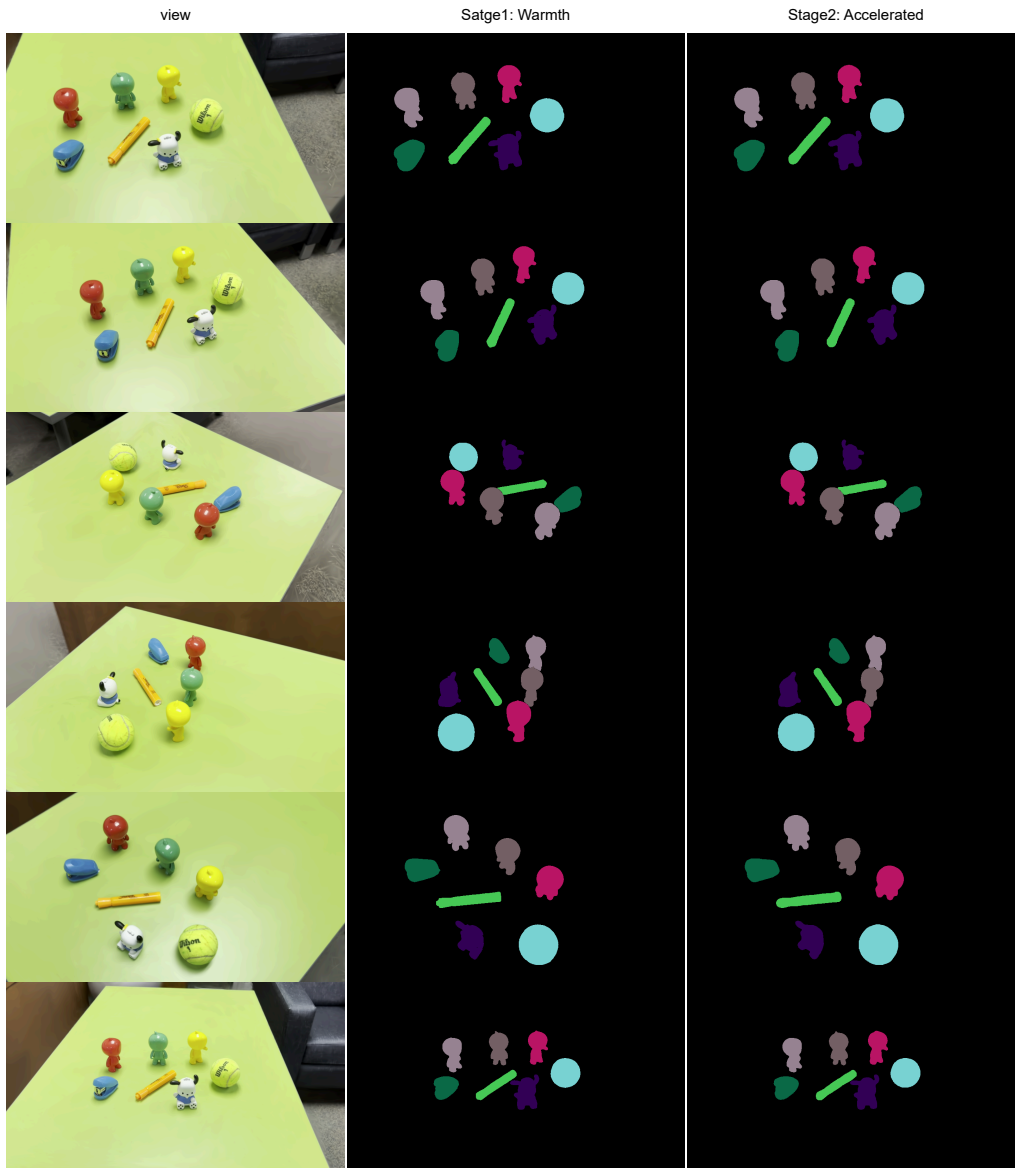


Figure 9: Comparison between Stage 1: Warm-Up and Stage 2: Accelerated. 1st col shows the rendering images, 2nd col shows the segmentation masks generated in Stage 1, and 3rd col shows the segmentation masks generated in Stage 2. (Different color indicate different objects.)

to perform rapid segmentation. Thus, theoretically, the segmentation capabilities of both stages are identical.

### C Limitations

The limitation of the SAGOnline algorithm is that it does not account for situations where a minority of Gaussian primitives contribute to multiple objects. The method of assigning a unique instance ID to each Gaussian primitive can lead to misclassification. As shown in Fig. 10, a small number of outliers appear at the boundaries between different instances, which affects the precision of the 3D mask for the Gaussian primitives.

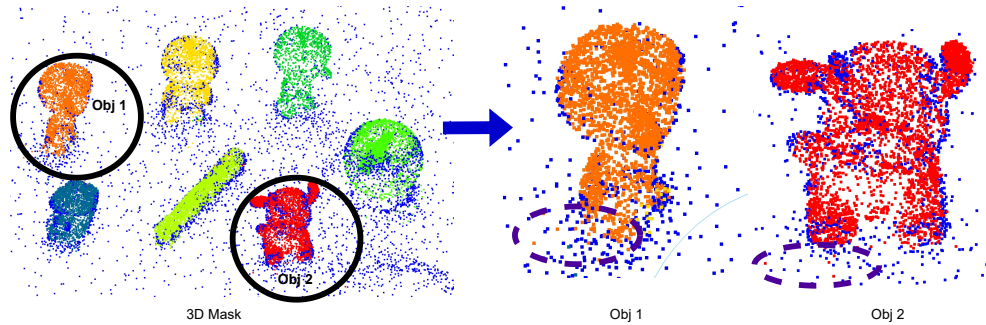


Figure 10: Limitation of SAGOnline. The left part shows the explicit effect of the 3D mask generated by SAGOnline on the Gaussian mean value points. Different colors represent different object instances, and the black circles highlight the instances with defective segmentation results. The right part presents enlarged images of the objects marked in the figure, with the dashed boxes highlighting the specific points that were inaccurately classified.

## D Broader Impacts

Our work enables efficient, multi-view consistent 3D instance segmentation in 3D Gaussian Splatting (3DGS) field, which carries significant societal implications:

### D.1 Positive Impacts

- **Augmented and Virtual Reality:** Enables real-time object manipulation in AR/VR applications, lowering barriers for content creation and interactive training systems.
- **Robotic Perception:** Improves 3D scene understanding for autonomous systems, potentially enhancing safety in dynamic environments (e.g., cluttered warehouses or roads).

### D.2 Potential Risks and Mitigations

- **Algorithmic Bias:** Performance may vary across object categories if training data is imbalanced. Transparency in dataset limitations is critical.
- **Environmental Cost:** While optimized, 3DGS still requires GPU resources. Future work should explore energy-efficient variants for edge devices.
- **Misuse Potential:** Malicious actors could exploit automated segmentation for 3D deepfakes. Code releases would include ethical use guidelines.

### D.3 Recommendations

We encourage:

- Interdisciplinary collaboration to address fairness and privacy in 3D scene understanding
- Benchmarking energy efficiency for real-world deployment
- Community efforts to diversify 3D segmentation datasets

This technology empowers creators and researchers while necessitating responsible development practices to maximize societal benefit.